Protein Structure and Folding:

Evf, a Virulence Factor Produced by the *Drosophila* Pathogen *Erwinia carotovora*, Is an *S*-Palmitoylated Protein with a New Fold That Binds to Lipid Vesicles

Sophie Quevillon-Cheruel, Nicolas Leulliot, Carlos Acosta Muniz, Michel Vincent, Jacques Gallay, Manuela Argentini, David Cornu, Frédéric Boccard, Bruno Lemaître and Herman van Tilbeurgh

J. Biol. Chem. 2009, 284:3552-3562.
doi: 10.1074/jbc.M808334200 originally published online November 1, 2008

THE JOURNAL OF BIOLOGICAL CHEMISTRY VOL. 284, NO. 6, pp. 3552–3562, February 6, 2009

Evf, a Virulence Factor Produced by the *Drosophila* Pathogen *Erwinia carotovora*, Is an *S*-Palmitoylated Protein with a New Fold That Binds to Lipid Vesicles*

Received for publication, October 31, 2008 Published, JBC Papers in Press, November 1, 2008, DOI 10.1074/jbc.M808334200

Sophie Quevillon-Cheruel[‡], Nicolas Leulliot[‡], Carlos Acosta Muniz[§], Michel Vincent[‡], Jacques Gallay[‡], Manuela Argentini[¶], David Cornu[¶], Frédéric Boccard[§], Bruno Lemaître[§1], and Herman van Tilbeurgh[‡2]

From the [‡]Institut de Biochimie et de Biophysique Moléculaire et Cellulaire, Université Paris-Sud, UMR8619-CNRS, IFR115, F-91405 Orsay, [§]Centre de Génétique Moléculaire, UPR-CNRS, 91190 Gif sur Yvette, and [¶]CNRS, Institut de Chimie des Substances Naturelles, Laboratoire de Spectrométrie de Masse, Imagif, UPR 2301, Av. de la Terrasse, 91198 Gif-sur-Yvette, France

Erwinia carotovora **are phytopathogenic Gram-negative bacteria of agronomic interest as these bacteria are responsible for fruit soft rot and use insects as dissemination vectors. The *Erwinia carotovora carotovora* strain 15 (*Ecc*15) is capable of persisting in the *Drosophila* gut by the sole action of one protein, *Erwinia* virulence factor (Evf). However, the precise function of Evf is elusive, and its sequence does not provide any indication as to its biochemical function. We have solved the 2.0-Å crystal structure of Evf and found a protein with a complex topology and a novel fold. The structure of Evf confirms that Evf is unlike any virulence factors known to date. Most remarkably, we identified palmitoic acid covalently bound to the totally conserved Cys^{209}, which provides important clues as to the function of Evf. Mutation of the palmitoic binding cysteine leads to a loss of virulence, proving that palmitoylation is at the heart of Evf infectivity and may be a membrane anchoring signal. Fluorescence studies of the sole tryptophan residue (Trp^{94}) demonstrated that Evf was indeed able to bind to model membranes containing negatively charged phospholipids and to promote their aggregation.**

Flies have been recurrently thought to be involved in the transmission of animal and plant diseases; they live on decaying medium enriched in micro-organisms, and they constitute ideal vectors for microbial dissemination through food contamination because of their close association with animals or plant communities. Although the potential hazard of flies on humans is generally accepted, the interactions between bacteria and potential fly vectors are poorly documented. Unlike the situation observed for plague bacteria and fleas (1) or for many protozoan parasites infecting humans and mosquitoes (2), in which the insect is an obligate host, little is known about the mechanisms that allow bacterial persistence within flies (3). The identification of one gene, the *Erwinia* virulence factor (Evf)[3] that promotes bacterial persistence in the gut of *Drosophila* larvae, has recently revealed the existence of specific strategies that may enhance survival of bacteria within insects and their dissemination in their environment.

The fruit fly *Drosophila melanogaster* lives in decaying fruits and has been occasionally implicated in the transmission of plant phytopathogens such as the enteric bacteria *Erwinia carotovora* (4, 5). *E. carotovora* species induce the soft rotting of many fruits and potatoes through the production of a battery of pectinolytic enzymes (6). A strain of *E. carotovora carotovora*, *Ecc*15, was identified that, contrary to most bacterial species, can persist in the gut of *Drosophila* larvae after natural ingestion (7). This infection relies on a very specific bacterium host interaction because only a very limited number of strains is capable of inducing this response. A genetic screen set up to search for infective genes revealed that infectivity is mediated by a single gene, *Erwinia* virulence factor (Evf) (8). The expression of Evf is regulated by Hor, a member of the family of transcriptional regulators of the SlyA type that are usually involved in the regulation of virulence genes (9). Evf is only present in a subset of *Erwinia* strains that have infectious properties and was characterized as a gene that promotes survival and dissemination (10). Strikingly, transfer of Evf into noninfectious, and normally nonpersistent, Gram-negative bacteria enables them to persist in the *Drosophila* gut and to elicit a systemic immune response.

The biochemical function of the Evf protein and the exact mechanism by which it promotes bacterial persistence in the gut remain unknown. However, it was shown that it does not function using previously well known mechanisms of bacterial survival. It does not act by directly counteracting the host immune response; it is not a toxin, and it does not provide protection against antibacterial peptides or against reactive oxygen species. The presence of Evf leads to the accumulation of bacteria in the anterior midgut and dramatically affects gut

* The costs of publication of this article were defrayed in part by the payment of page charges. This article must therefore be hereby marked "*advertisement*" in accordance with 18 U.S.C. Section 1734 solely to indicate this fact.

The atomic coordinates and structure factors (code 2W3Y) have been deposited in the Protein Data Bank, Research Collaboratory for Structural Bioinformatics, Rutgers University, New Brunswick, NJ (http://www.rcsb.org/).

[1] Present address: School of Life Sciences, Ecole Polytechnique Fédérale de Lausanne, CH-1015 Lausanne, Switzerland.

[2] To whom correspondence should be addressed. E-mail: herman.van-tilbeurgh@u-psud.fr.

[3] The abbreviations used are: Evf, *Erwinia* virulence factor; MALDI-TOF, matrix-assisted laser desorption ionization time-of-flight; ESI-MS, electrospray ionization-mass spectrometry; LC-MS/MS, liquid chromatography-tandem mass spectrometry; PC, phosphatidylcholine; POPS, 1-palmitoyl-2-oleoyl-*sn*-glycero-3-phosphoserine; DTT, dithiothreitol; SUV, small unilamellar vesicle; Bicine, *N*,*N*-bis(2-hydroxyethyl)glycine; r.m.s.d., root mean square deviation.

physiology (10). Evf therefore reveals a new aspect of bacterial strategies for colonizing an insect gut niche. Interestingly, *Ecc*15 accumulated in the infected gut in a nonrandom arrangement reminiscent of biofilms, which might allow the bacteria to interfere with gut peristalsis and therefore prevent elimination by passive transfer through the gut. Biofilm formation in the gut preventing normal blood feeding is also seen in the infection of the flea vector by *Yersinia pestis* (11). Evf has few orthologues in other bacteria and no identified functional sequence signatures. Interestingly, the closest homologue is a gene from *Photorhabdus luminescens*, a bacterium that exists in symbiosis in the guts of nematodes (12) suggesting that Evf-like proteins are also virulence factors that promote specific interaction with the host gut allowing persistence.

To better understand the function of the Evf protein at the molecular level, we have determined its crystal structure. We show that Evf is an α/β protein with a complex topology and a novel fold. Most remarkably, the crystal structure and mass spectrometry data clearly demonstrate that a palmitoic acid is covalently linked to the 209 cysteine residue via a thioester linkage. To assess whether the association of Evf with palmitoic acid is necessary for infection, mutations of this cysteine residue into alanine or serine were tested for infectivity. All mutants lacking the palmitoic acid-bound residue did not give rise to an immune reaction. We also showed that Evf interacted with model membranes and was able to promote their aggregation. We postulate that the palmitoyl moiety might play a role in these membrane-associated processes.

MATERIALS AND METHODS

Cloning, Expression, Purification, and Labeling—Evf was amplified by PCR using the plasmid pOM1-evf as a template (7). An additional sequence coding for a 6- histidine tag was introduced at the 3′ end of the gene during amplification. The PCR product was then cloned into a derivative of the pET9 vector. Expression was done at 37 °C during 3 h using the transformed *Escherichia coli* BL21-Gold(DE3) strain (Novagen) and 2× YT medium (Bio 101, Inc., Vista, CA). When the cell culture reached an A_{600} nm of 1, protein expression was induced with 0.5 mM isopropyl 1-thio-β-D-galactopyranoside (Sigma), and the cells were grown for a further 4 h. Cells were harvested by centrifugation, resuspended in 40 ml of 20 mM Tris-HCl, pH 7.5, 200 mM NaCl, 5 mM β-mercaptoethanol, and stored overnight at −20 °C. Cell lysis was completed by sonication. The His-tagged protein was purified on a nickel-nitrilotriacetic acid column (Qiagen), eluted with imidazole, and loaded on to a Superdex^{TM} 200 column (Amersham Biosciences), equilibrated against 20 mM Tris-HCl, pH 7.5, 200 mM NaCl, 10 mM β-mercaptoethanol. Selenomethionine-labeled protein was prepared as described and purified as the native protein (13). The homogeneity and selenomethionine labeling of the proteins were checked by SDS-PAGE mass spectrometry. The covalent palmitoylation of Cys^{209}, as suggested by analysis of the crystal structure, was verified by mass spectrometry. All spectra were acquired in positive-ion mode on a Voyager DE-STR MALDI-TOF mass spectrometer (Applied Biosystems, Foster City, CA) equipped with a 337-nm nitrogen laser. Determinations of the molecular masses of Evf proteins were performed in linear mode (accelerating voltage, 25 kV; grid voltage, 93%; guide wire, 0.3%; delay, 600 ns) with external calibration using sinapinic acid as matrix.

TABLE 1
Data collection and refinement statistics

Protein	Evf selenomethionine
Space group	$P2_12_12_1$
Unit cell parameters *a, b, c*	69.5 Å, 86.7 Å, 91.4 Å
Resolution	80.0-2.0 Å
Total no. of reflections	1,056,433
Total no. of unique reflections	38,113
Multiplicity	27.7
R_{merge}[a]	9.6
$I/\sigma(I)$	25.9
Overall completeness (%)	100
R/R_{free} (%)	20.1/24.9
R.m.s.d. bonds	0.011 Å
R.m.s.d. angles	1.181°
Ramachandran plot	
Disallowed	0.4
Most favored	5.5
Allowed	94.1

[a] $R_{merge} = \Sigma_h\Sigma_i|I_{hi} - \langle I_h\rangle|/\Sigma_h\Sigma_i I_{hi}$, where I_{hi} is the ith observation of the reflection h, and $\langle I_h\rangle$ is the mean intensity of reflection h.

Crystallization, Data Collection, Structure Solution, and Refinement—Crystals of both the native and selenomethionine-labeled protein were grown from a 1:1 μl mixture of protein (10 mg/ml) with 25% PEG4000, 50 mM Bicine, pH 8, 0.1 mg/ml trypsin. The addition of trypsin resulted in *in situ* limited proteolysis and was necessary for crystal formation.

X-ray diffraction data from a crystal of the selenomethionine-substituted protein were collected on beamline ID23-1 (European Synchrotron Radiation Facility) at a single wavelength of 0.9798 Å, corresponding to the peak position of the selenium *K*-edge to optimize the anomalous scattering signal strength. The crystals belong to space group $P2_12_12_1$ with two Evf copies per asymmetric unit, corresponding to 40% solvent content. Data processing was carried out with the programs MOSFLM (14) and SCALA (15). The cell parameters and data collection statistics are reported in Table 1. A total of 720 frames of 1° rotation were collected on a single crystal with an attenuated beam, with no evidence of overall radiation damage. Because of the high redundancy, the two selenium atoms were readily localized using the Hyss module of PHENIX (16). Phasing was performed using Sharp (17). A high resolution dataset was recorded on the same crystal without any attenuation. The program SOLOMON (18) was used for density modification using the phases from Sharp, and the resulting phases were transferred into the high resolution dataset. A combination of Arp/warp (19) and Resolve (20) was able to build 90% of the structure. Further rebuilding and refinement of the model were performed with O (21) and refined with REFMAC (22).

Sample Preparation and Mass Spectrometry Measurements—For ESI-MS measurements, 20 μl of purified Evf protein (4.5 μg/μl) was desalted with size exclusion chromatography columns (Micro Bio-Spin 6 chromatography columns, Bio-Rad), following the manufacturer's recommendations, and eluted in water. Ten μl of desalted Evf protein was mixed with the same volume of acetonitrile (100%) and DTT (10 mM). The reaction was left to proceed for 20 min at 56 °C and then 1% of formic acid was added. Desalted protein samples were loaded into nanoelectrospray needles (Proxeon Biosystems A/S, catalogue

number ES 388). Positive ion ESI mass spectra were acquired using a QTOF Premier mass spectrometer (Waters). The instrument was mass-calibrated by spraying a solution of sodium iodide (2 μg/μl). The ion source parameters were as follows: capillary voltage 1.4 kV, cone voltage 40 V, ion source block temperature 80 °C, nebulizer gas flow 25 liters/h. The mass spectra were analyzed using the MassLynx software (Waters) and deconvoluted using the MaxEnt 1 algorithm.

For nanoLC-MS/MS analyses, 1 μl of purified Evf protein (4.5 μg/μl) was diluted in 10 μl of 20% acetonitrile, 80% 50 mM NH_4HCO_3 and enzymatically digested with bovine trypsin or *Pseudomonas fragi* Asp-N (both purchased from Roche Applied Science) with an enzyme/protein ratio of 1/45 (w/w). The digestion was left to proceed for 4 h at 37 °C. When reduction/alkylation reactions were performed, DTT and iodoacetamide were added after protein dilution at a final concentration of 5 and 18 mM, respectively. DTT was first added for 20 min, and then iodoacetamide was added and left to react for 30 min in the dark at room temperature. Peptide mixtures were Speed-Vac-treated for 10 min and then analyzed with the QTOF Premier mass spectrometer coupled to the Acquity nano-UPLC equipped with a trapping column (Symmetry C18, 180 μm × 20 mm, 5-μm particle size) and an analytical column (BEH130 C18, 75 μm × 100 mm, 1.7-μm particle size) (Waters). The aqueous solvent (buffer A) was 0.1% formic acid in water, and the organic phase (buffer B) was 0.1% formic acid in acetonitrile. A 2–40% B gradient was set for 25 min. Mass spectrometer parameters were as described previously for ESI-MS measurements except for capillary voltage (3 kV) and collision energy (ramping from 15 to 40 eV). For exact mass measurements, Glu-fibrinopeptide reference (m/z = 785.8426) was continuously supplied during nanoLC-MS/MS experiments using the lockspray device. Peptide mass measurements were finally corrected by ProteinLynx Global Server, (Waters) during data processing. Peak lists were generated by ProteinLynx Global Server, and processed data were submitted to searching using the following parameters: data bank His-tagged Evf protein; peptide tolerance 15 ppm; fragment tolerance 0.1 Da; digest reagent trypsin or Asp-N; variable modifications oxidation (methionine) and palmitoylation (cysteine, Serine); fixed modifications carbamido-methylation (cysteine).

For MALDI-MS analyses, peptide extracts (0.5 μl) were mixed with an equal volume of 2,5-dihydroxybenzoic acid (10 mg/ml) or α-cyano-4-hydroxycinnamic acid (10 mg/ml) matrix compounds (Sigma). MALDI-MS measurements were carried out on a Voyager-DE STR MALDI-TOF mass spectrometer (Applied Biosystems) in the positive ion reflectron mode. Peak lists were generated by the Data Explorer software (Applied Biosystems), and processed data were submitted to the Find-Mod and Findpep software using the already described parameters except for tolerance at 50 ppm.

Steady-state Fluorescence Measurements—Fluorescence emission spectra were recorded with a home-modified SLM spectrofluorimeter with slit width of 4 nm for excitation and 8 nm for emission. Excitation was vertically polarized, and the emission was detected through a polarizer oriented at the magic angle 55°. Measurements were performed in 100-μl microcuvettes.

Time-resolved Fluorescence Measurements—Fluorescence intensity and anisotropy decays were obtained from the polarized $I_{vv}(t)$ and $I_{vh}(t)$ components measured by the time-correlated single-photon counting technique. A light-emitting diode (PLS 295, serial number PLS-8-2-237 from Picoquant, Berlin-Adlershof, Germany) (maximal emission at 298 nm) operating at 10 MHz was used as excitation source. A short pass Asahi Spectra UV filter ZUS300 was used in front of the LED. A Hamamatsu fast photomultiplier (model R3235-01) was used for detection. Emission wavelength was selected through a Omega 320AELP cutoff filter and a Oriel bandpass filter UG5-005FG09-50S. Fluorescence intensity decay analyses were performed with the maximum entropy method (23), using a multiexponential model, $\sum_i \alpha_i \exp(-t/\tau_i)$, as described previously. A classical anisotropy model, $A(t) = \sum_i \beta_i \exp(-t/\theta_i)$, in which any rotational correlation time (θ) is coupled with each lifetime (τ), was used to resolve polarized fluorescence decays (24). The amplitude of the internal rotation, ω_{max}, was calculated according to the wobbling-in-cone model (25).

Preparation of Sonicated Phospholipid Vesicles—The phospholipid suspensions were prepared by sonication using egg PC and POPS (both from Avanti Polar Lipids, Alabaster, AL) dissolved in chloroform. The organic solution was evaporated to dryness in a glass tube under a stream of nitrogen. Remaining traces of organic solvent were further removed by submitting the sample to high vacuum during several hours. Hydration of the sample was achieved with either 20 mM Hepes buffer, pH 7.2, or 100 mM cacodylate buffer, pH 5. After vortexing, the multilamellar vesicles formed were sonicated at room temperature with the micro-tip of a Branson-B12 sonifier during 5 min with half-duty cycles.

Drosophila Strain and Natural Bacterial Infection—A transgenic strain carrying a diptericin-*lacZ* was used to monitor the immune response of larvae. Diptericin-*lacZ* is a *P* transgene containing a fusion between 2.2 kb of upstream sequence of the antibacterial peptide gene diptericin and the β-galactosidase gene (26). Approximately 200 third-instar larvae were placed in a 2-ml tube containing 200 μl of concentrated bacteria pellet (A_{600} = 200) from an overnight culture and 400 μl of crushed banana. The larvae, bacteria, and banana were thoroughly mixed in the microcentrifuge tube; the tube was closed with a foam plug, incubated at room temperature for 30 min, and the mixtures then transferred to a standard cornmeal fly medium and incubated at 29 °C. LacZ titration was performed as described (27).

Bacterial Strains—The strains and plasmids used in this study are listed in Table 2. Bacteria were cultured in Lennox medium with the appropriate antibiotics (100 μg/ml rifampicin; 100 μg/ml spectinomycin). The rifampicin-resistant *Ecc*15 and *Ecc*15 derivatives were grown at 29 °C. *E. coli* strains were grown at 37 °C.

Constructions of Evf Derivatives EvfC209S and EvfC209A—The KpnI-HindIII fragment of plasmid pOM1-evf was replaced by KpnI-HindIII PCR fragments generated by using as template pOM1-evf and as primers one oligonucleotide overlapping the KpnI site and converting Cys^{209} into Ser^{209} (oligonucleotide S1, 5′-ATCGACGGTACCCATTTCAAGCAGGAGCAAAAGA-AGATCGCTACCTCTTCTGCTTCATATCAAGAAGTAA-

TABLE 2
Bacterial strains and plasmids

Strains and plasmids	Description	Source or Ref.
Bacterial strains		
E. carotovora 15 (*Ecc*15)	Wild type	8
*Ecc*15 *evf*	Evf::Tn*10* (Kan^R)	8
E. coli K12 MG1655	Wild type	Lab collection
Plasmids		
pOM1	Cloning vector pSC101 derivative (Spc^R)	49
pOM1-evf	pOM1 expressing *evf*	8
pOM1-evf (C209S)	pOM1 expressing *evf* (C209S)	This study
pOM1-evf (C209A)	pOM1 expressing *evf* (C209A)	This study

3′) or into Ala^{209} (oligonucleotide A1, 5′-ATCGACGGTACCCATTTCAAGCAGGAGCAAAAGAAGATCGCTACCTCTGCTGCTTCATATCAAGAAGTAA-3′) and one oligonucleotide overlapping the HindIII site.

RESULTS

Structure Determination and Quality—The full-length Evf protein failed to crystallize. To help crystallization, we have screened crystallization conditions of the Evf protein in presence of trypsin protease. This may enable unstructured regions to be proteolyzed, thereby providing a truncated construct more suitable for crystal formation. This is an often used strategy for obtaining or improving crystals, but usually the truncated construct is further purified to remove the protease. We opted for a different strategy that consists of directly adding the protease to the crystallization drops. In our strategy, the nature and concentration of the protease are used as variable parameters in the crystallization screen. The idea is to provoke proteolysis directly under physicochemical conditions where crystals of the truncated product can nucleate. This strategy has been applied successfully in a number of projects in our laboratory (28, 29). Once a crystal hit was found, all the subsequent optimizations were performed with the protease present in the crystallization drop. The effect of the protease on crystallogenesis is discussed further.

The structure of Evf was solved by single anomalous dispersion using selenomethionine-labeled protein. The presence of only two methionines (excluding the N-terminal methionine) for a total of 270 residues made the detection of the selenium sites challenging. Fortunately, the weakness of the anomalous signal was compensated by the high resistance of the crystals in the x-ray beam, which enabled a highly redundant dataset to be collected. The final model contains residues 8–19 and 24–277 for one chain and residues 10–19 and 27–277 for the other. The two copies of Evf have identical structures (r.m.s.d. 0.38 Å). Refinement statistics are gathered in Table 1 and show good stereochemistry for the final model.

Evf Structure Reveals a Novel Fold—The Evf protein adopts a globular fold with approximate dimensions 60 × 50 × 25 Å. The Evf protein contains two 3_{10} helices (H1 and H2), six α-helices (α1 to α6), and 10 β-stands (β1 to β10) with a fairly complex topology (Fig. 1*A*, generated using Tops (30)). A search in the EBI-SSM server found no proteins with a similar fold in the Protein Data Bank. The Evf protein structure is therefore the first representative of a novel protein fold family.

The Evf fold can be described as a central mixed β-sheet sandwiched between two α-helical layers (Fig. 1, *B* and *C*). The six-stranded β-sheet contains four antiparallel strands (β6β7β8β3/β4) which is completed after β6 by strand β2 and β1 from the N terminus of the protein and β9 from the C terminus as follows: β2 follows β6 and the β1 and β9 strands both form the last "strand" of the β-sheet, respectively, anti-parallel and parallel to β2.

The β-sheet is highly curved and forms a half-barrel that cradles one of the α-helices (α4), a structural trait reminiscent of the fold seen in proteins of the hot-dog and related families (31, 32). The helical domain packing on the exterior convex side of the β-sheet is composed of the α1 at the N terminus, the α2, H1 and α3 helices (inserted between β2 and β3), and the α6 and α7 helices (inserted between β8 and β9). The α2 and α3 helices pack on the β-sheet roughly parallel to the β-strands, whereas α1 and α7 pack on the α2 and α3 helices at an ~20° angle. Although this helical cap seems to form an independent structural domain, it contains elements from the N and C terminus of the protein. The second α-helical layer on the concave side of the β-sheet is composed of the α4 and α5 helices (inserted between β4 and β6) and the H2 3_{10} helix (inserted between β7 and β8). The α4 helix runs inside the half-β-barrel, whereas α5 and H2 are perpendicular to the barrel axis and form a "lid" over the side of the barrel.

In Situ Proteolysis during Crystallogenesis—As the protein only crystallized in the presence of trypsin, we set out to identify the crystallized Evf fragment. Mass spectrometry and Edman sequencing of dissolved crystals proved that Evf was cleaved at Arg^{23}. Surprisingly, the electron density maps clearly showed that the peptide between residues 8 and 19 was present and well defined in the crystal structure forming helix α1 and flanking residues. The seven N-terminal residues up to the beginning of helix α1 and the three residues after α1 (Pro^{20}–Gly^{22}) in the α1-β1 loop were not visible in the final electron density map and were therefore not modeled. Trypsin digestion led to cleavage of the polypeptide chain at Arg^{23}, and the residues from the N terminus and from the cut α1-β1 loop are probably disordered. It therefore appears that digestion of the protein by trypsin did not help crystallization by providing a shorter construct but simply by cutting inside the α1-β1 loop. Contrary to the residues 30–36 before β1, which pack against the side of the protein and have *B*-factors comparable with the rest of the protein residues, residues 23–29 protrude more into the solvent and have higher *B*-factors suggesting that residues 20–29 form a mobile loop. In our structure, the distance between Gly^{19} and Arg^{23} is compatible with the modeling of the three missing residues, but the cut most probably relaxes the structure of the loop away from a conformation that hampers crystallization. Inspection of the crystal packing indeed shows that this region is involved in intermolecular contacts, which could have been hindered with the intact protein. Addition of the protease therefore acts as a surface engineering step rather that removing unstructured regions.

Evf Is S-Palmitoylated on Cys^{209}—During refinement, clear residual electron density was detected indicating the presence of a long chain ligand covalently linked to Cys^{209} (Fig. 2). The hydrophobic nature of the surrounding residues and the form

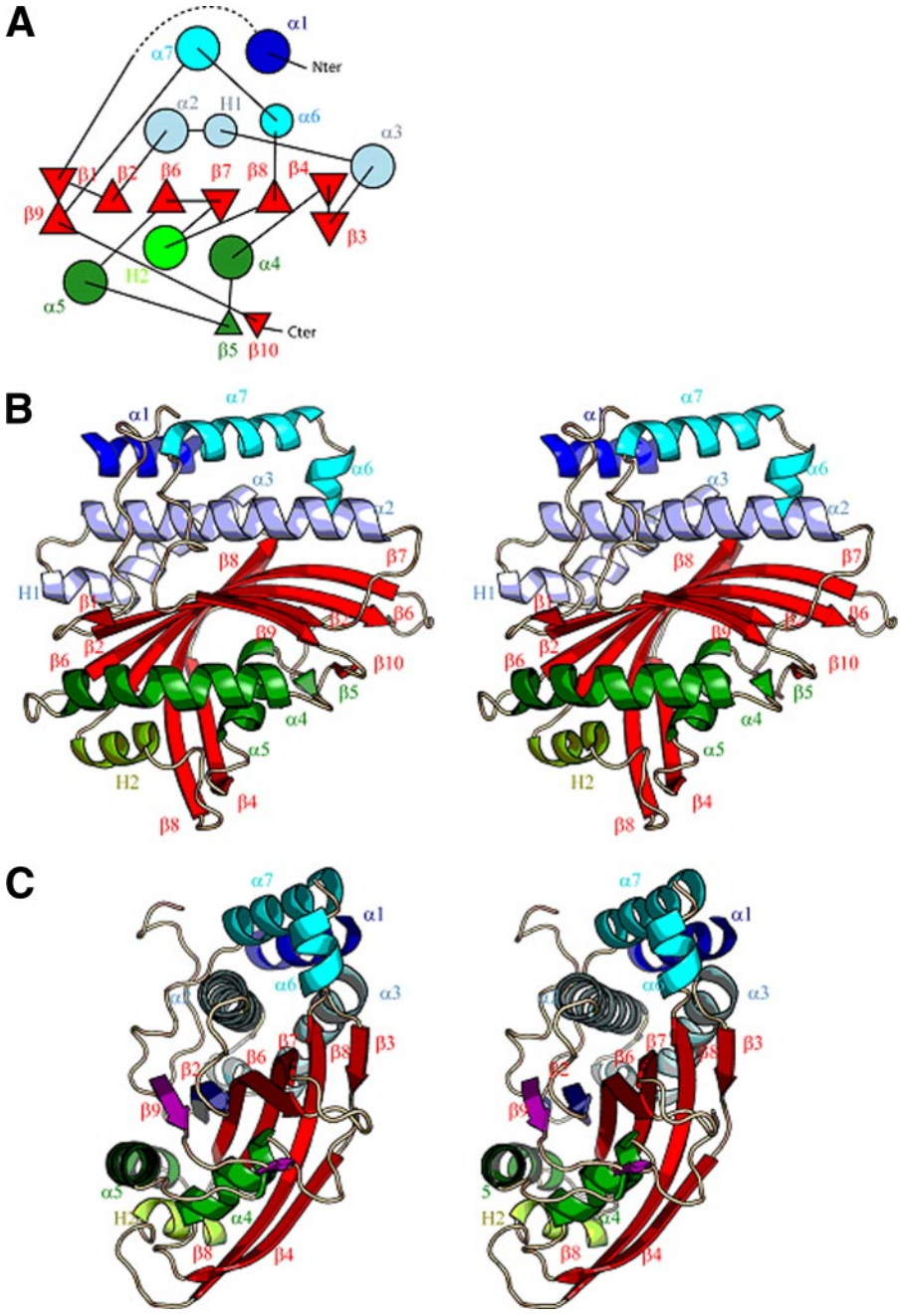

FIGURE 1. **Structure of Evf.** *A*, topology diagram of Evf. Helices (*circles*) and strands (*triangles*) are colored using the same code as in *B*. *B*, schematic stereographic presentation of Evf. *C*, same as *B* rotated 90°.

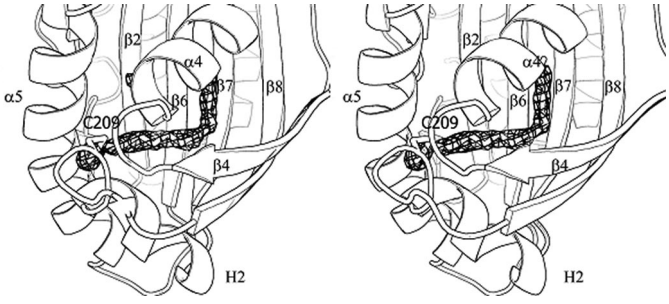

FIGURE 2. **Covalent lipid binding to Evf.** Palmitoic acid-binding site of Evf. The lipid forms a thioester bond with Cys[209]. The electron density of the residual $F_o - F_c$ map contoured at 3σ is shown in *mesh* generated with the palmitoic acid excluded from the model.

of the electron density suggested that a fatty acid was bound. To gain insight into the chemical nature of the fatty acid, direct ESI-MS measurements of the desalted Evf protein with and without DTT treatment were performed. Note that DTT-induced chemical reduction was left to proceed under denaturing conditions (see "Materials and Methods"). The ESI-MS deconvoluted mass spectra are shown in Fig. 3*A*. Without DTT treatment, the Evf measured mass was 32,469.8 Da, whereas the expected mass was 32,236 Da (mass shift = 233.8). Mass accuracy was 2 Da as evaluated by ESI-MS measurements of standard proteins (data not shown). Remarkably, DTT treatment caused the appearance of a supplementary peak at 32,232.7 Da (mass shift = −237.9), in addition to the peak corresponding to the Evf protein (32,470.6 Da). These results indicate that DTT, under denaturing conditions, can efficiently reduce the Evf amino acid that most probably harbors a palmitoyl group (expected mass shift = 238).

To confirm that palmitoylation happens on Cys[209], peptide mixtures generated by in-solution enzymatic digestion were submitted to nanoLC-MS/MS and MALDI-MS analyses. After trypsin and Asp-N enzymatic digestion, a total sequence coverage of 90% was reached (Fig. 3*B*), and similar results were obtained after in-gel digestion (data not shown). Average mass accuracy was 10 ppm. The two Evf amino acidic regions were not covered by either nanoLC-MS/MS or by MALDI-MS analyses (*boxed peptides* in Fig. 3*B*). The 55–64-amino acid sequence was not covered probably because in that region trypsin and Asp-N endoproteases are unable to generate peptides with compatible length for mass spectrometry analyses. In contrast, the absence of detection for the 205–221-amino acid Evf peptide (harboring Cys[209]) was somehow intriguing. DTT reduction followed by iodoacetamide alkylation was performed prior to Evf trypsin digestion, and nanoLC-MS/MS analyses allowed us to efficiently detect and fragment the carbamidomethylated 205–221-amino acid Evf peptide thus confirming its sequence (data not shown). These results indicate that, before alkylation, DTT efficiently reduces Cys[209] most probably eliminating the palmitoyl group. Hence, solubilization and/or ionization of the 205–

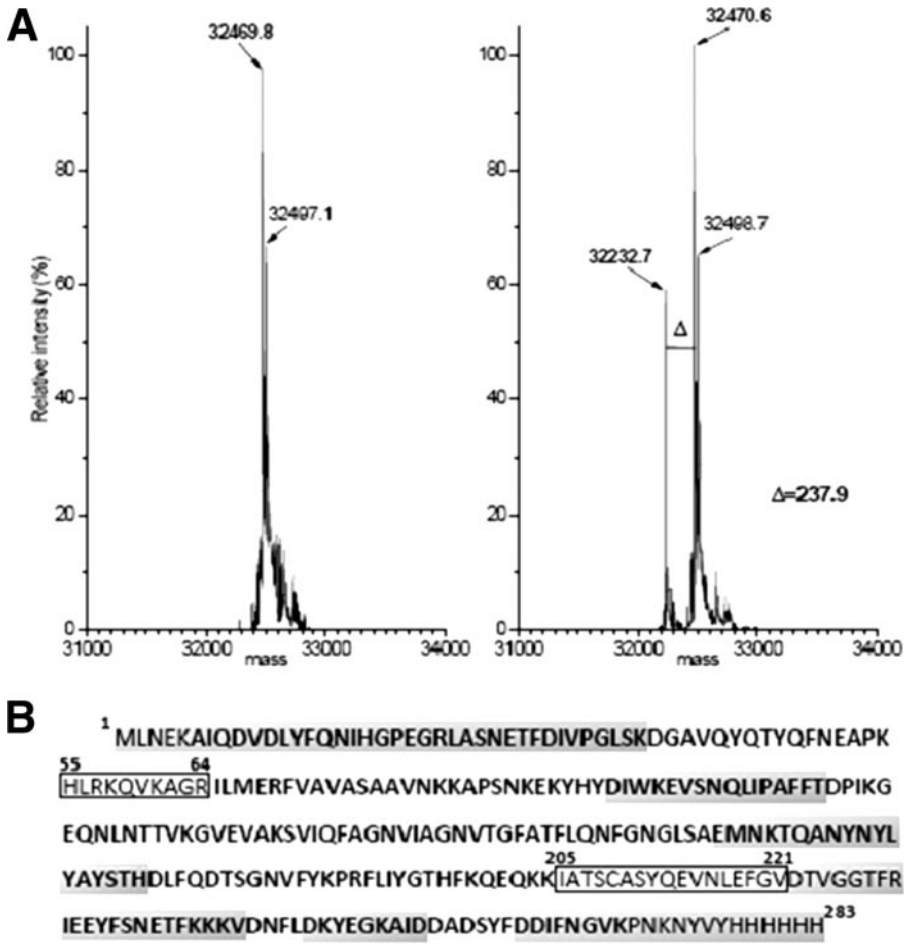

FIGURE 3. **Mass spectrometry analysis reveals the presence of a palmitoyl group covalently bound to Evf.** *A,* deconvoluted ESI mass spectra of intact Evf with and without DTT treatment are presented. The positive ion mass spectra were acquired from $m/z = 350$ to $m/z = 2000$ and then deconvoluted. DTT-induced reduction allows the loss of a palmitoyl group from the Evf protein ($\Delta = 237.9$). The 32,497.1 and 32,498.7 peaks could correspond to oxidized forms of the native Evf protein ($\Delta = 18$). *B,* amino acid sequence of initially expressed Evf is reported. Detected and fragmented Evf peptides are shown: tryptic peptides are in *boldface* and Asp-N generated peptides are *shaded*. *Boxed* sequences were not detected under standard conditions (without DTT/iodoacetamide treatment).

221-amino acid Evf peptide could be disturbed by the presence of the palmitoyl group.

Crystal structure data corroborate the mass spectrometry results. Indeed, the palmitoyl group perfectly accommodates into the residual electron density connected to Cys^{209}. The crystallographic *B*-factors of the palmitoyl are of the same order as surrounding residues, indicating a high level of occupation of this ligand in the crystallized protein. The palmitoyl moiety is covalently linked via a thioester linkage to the sulfur group of the side chain of Cys^{209}, situated at the exit of helix H2 (Fig. 2). The aliphatic chain is totally buried in a hydrophobic shaft formed by the central β-sheet and the α4-helix (Fig. 2). The cavity is topped by the H2 and α5-helices. The fatty acid-binding cavity is lined exclusively by hydrophobic residues as follows: Leu^{116}, Val^{125}, Val^{129}, Phe^{132}, Ala^{133}, Leu^{155}, Tyr^{170}, Phe^{198}, Ile^{205}, Phe^{219}, and Val^{221}.

Palmitoylation Is Necessary for Infectivity—Psi-BLAST search retrieved three homologous Evf sequences, and the alignment is represented in Fig. 4. Two homologues are from nitrogen-fixing bacterial symbionts of legumes (*Rhizobium leguminosarum* and *Sinorhizobium medicae*; both have 18% sequence identity), which are of great importance in agriculture because of their role in converting atmospheric nitrogen into ammonia that is utilized by the plant. The other is from *P. lumeniscens* (25% sequence identity with Evf), an insect pathogen that lives in a symbiotic relationship within the guts of entomopathogenic *Heterorhabditid* nematodes. Despite weak sequence identities, analysis of the sequence against the structure of Evf leads to the conclusion that the four orthologues probably adopt the same fold. Most interestingly, the palmitoylated cysteine (Cys^{209}) is absolutely conserved in all of them. The hydrophobic nature of the residues lining the fatty acid cavity is also perfectly preserved, and therefore, covalent fatty acid attachment seems plausible in all orthologues (Fig. 4).

The total conservation and covalent modification of Cys^{209} suggested that this residue might be important for biological function. To assess the importance of Cys^{209}, we have used the property that upon transformation with the *evf* gene, *E. coli* or an *Ecc*15 *evf* mutant (evf^-) becomes infectious and persists in the gut of *Drosophila* and activates the expression of antibacterial peptide genes such as diptericin in the fat body. We have analyzed the infectivity of *E. coli* and *Erwinia* strains carrying the plasmids pOM-evf(C209S) and pOM-evf(C209A) in which Cys^{209} was mutated into a serine and alanine, respectively. A Western blot shows that bacteria expressed the mutated protein albeit at a lower level than bacteria carrying the pOM-evf plasmid expressing the wild-type protein. The level was, however, similar to the endogenous level expressed by the *Ecc*15 strain. We used these bacteria to infect *Drosophila* larvae containing a diptericin-*lacZ* reporter gene. Fig. 5 shows that *Ecc*15 as well as *E. coli* or *Ecc*15 evf^- expressing the wild-type form of Evf activate a strong expression of the immune gene reporter demonstrating their capacity to persist and activate an immune response. Importantly, neither *E. coli* nor *E. carotovora* carrying a plasmid producing an Evf variant mutated in the palmitoylation site activates an immune response. Use of green fluorescent protein-labeled bacteria reveals that bacteria expressing the mutated form of Evf did not persist in the gut (data not shown). Because these mutants are chemically incapable of being *S*-acylated, these results suggest that palmitoylation at Cys^{209} may be crucial for biological activity.

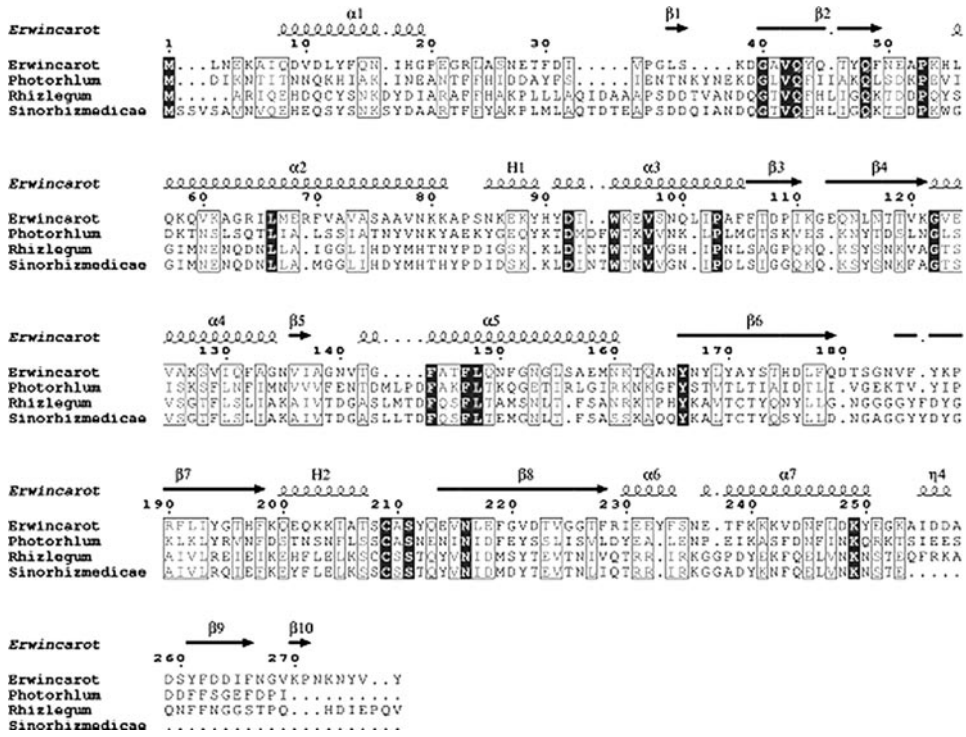

FIGURE 4. **Sequence alignment of Evf orthologues.** Alignment of sequences of Evf orthologues. The present Evf secondary structure elements are superposed on the sequence. The figure was generated using ESPRIPT (50).

Evf Interacts with Membranes and Promotes Their Aggregation—The presence of a fatty acid moiety covalently attached to Evf and the phenotypic effects of the Cys^{209} mutant led us to assume that it could serve as a membrane anchoring signal as described for other lipidated proteins (33, 34). Since we presently ignored the nature of the hypothetical membrane targeted by Evf, we studied binding to model membranes with different lipid composition and at different pH values. We have tested this hypothesis using SUV model membranes. Both electrostatic and hydrophobic interactions can be involved in protein-membrane interactions. We investigated their respective existence with either zwitterionic membrane vesicles constituted of egg phosphatidylcholine or negatively charged membrane vesicles made of mixtures of this phospholipid with the negatively charged phosphatidylserine. Phosphatidylcholine is a major membrane phospholipid, whereas phosphatidylserine is present in apoptotic membranes. We performed measurements both at neutral pH (pH 7.2) and in mild acidic conditions (pH 5) to amplify potential electrostatic interactions. We estimate that these pH values are close to those of physiological conditions. We used the fluorescence signal of the single tryptophan residue of Evf (Trp^{94}) to report the binding of the protein to the vesicles. The fluorescence emission spectrum of Evf in solution peaked at ~325 nm (Fig. 6), at both pH values, indicating a hydrophobic environment for its tryptophan. The three-dimensional structure indeed shows that Trp^{94} is part of the hydrophobic core of the protein and is situated close to but not in direct contact with the palmitoyl group. The fluorescence maximum remained unchanged upon Evf binding to membrane vesicles (Fig. 6, *A* and *B*). The fluorescence intensity decreased progressively by 35% upon egg PC-SUV addition at neutral pH (Fig. 6*A*, *inset*), indicating the involvement of hydrophobic interactions in the binding process. The existence of electrostatic interactions was shown by the enhanced effect observed when vesicles containing POPS (egg PC/POPS 9/1) were used; the fluorescence intensity decrease was steeper and larger than with PC alone (Fig. 6*A*, *inset*). Increasing the POPS content to 20% mol fraction did not change the results (not shown). The extent of fluorescence quenching was larger in mild acidic conditions (pH 5) than at neutral pH (Fig. 6*B*, *inset*). However, NaCl addition on Evf-membrane preformed complex did not reverse the interaction in both pH conditions (Fig. 6, *A* and *B*, *empty squares*). Overall, this set of data showed that both hydrophobic and electrostatic interactions participate in Evf binding to the membranes.

Excited-state lifetime measurements showed that the observed fluorescence quenching provoked by membrane binding was because of an increase of the contribution of a short lifetime population, decreasing the amplitude average excited state lifetime at both pH values (Fig. 7 shows the results at pH 7.2). This indicated a conformational change of the protein leading to an increase of the local flexibility around the tryptophan residue upon membrane binding at both pH.

In this respect, fluorescence anisotropy decay measurements allow obtaining information on the Trp rotational motion. Only one rotational correlation time was systematically detected, because of the instrument limits, corresponding to the Brownian nanosecond rotational motion of the protein (Table 3). Internal subnanosecond rotations were nevertheless likely because the experimental initial anisotropy value (β, Table 3) was significantly lower than that of the limiting anisotropy $A_0 = 0.251$, measured in the absence of rotational motion (35). The angular range of the subnanosecond rotation of the tryptophan residue, ω_{max}, calculated according to the wobbling-in-cone model (25, 36), increased significantly upon binding of the protein to SUV (Table 3). This flexibility increase was larger at pH 5 than at pH 7.2. Compared with its state at pH 7.2, the unbound protein was more compact at pH 5 (smaller Brownian rotational correlation time and smaller ω_{max} value) but became more flexible in the membrane-bound state.

Evf was not only able to bind to membranes but also promoted their aggregation at pH 5 as shown by turbidity measurements. Addition of Evf to SUV instantaneously increased the absorbance at 340 nm (Fig. 8). The essential electrostatic nature of the process was demonstrated by its very weak amplitude at pH 7.2 and its reversibility at pH 5 upon ionic strength increases (Fig. 8).

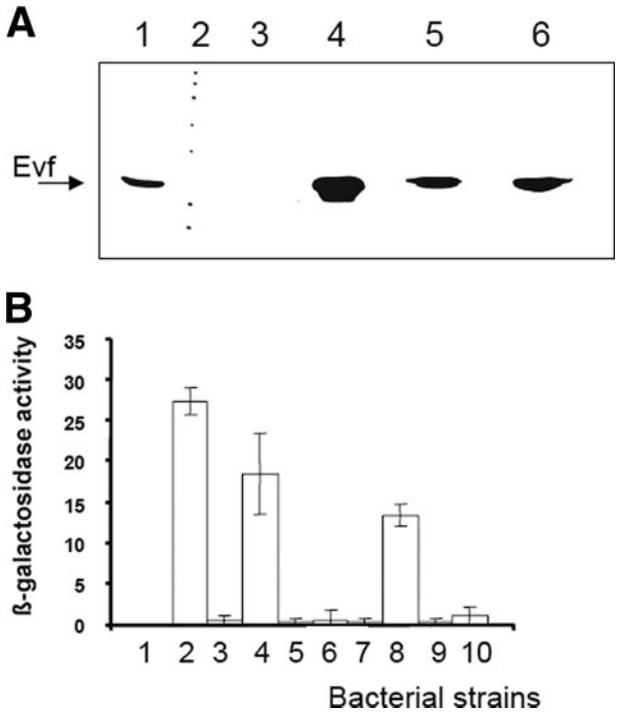

FIGURE 5. **Mutation in the site of palmitoylation abolishes the activity of Evf.** *A,* Western blot analysis with protein extracts derived from the following bacteria strains: *lane 1, Ecc*15 pOM1; *lane 2,* size marker; *lane 3, Ecc*15 *evf*⁻ pOM1; *lane 4, Ecc*15 *evf*⁻ pOM1-*evf*; *lane 5, Ecc*15 *evf*⁻ pOM1-evf(C209S) and *lane 6, Ecc*15 *evf*⁻ pOM1-evf(C209A). Evf proteins mutated in the palmitoylation site (Cys^{209}) accumulated at a lower level that the wild-type counterpart. However, the level of protein was higher than the endogenous level of Evf in the wild-type strain *Ecc*15. Evf was detected using rabbit polyclonal antibodies directed against the whole protein. *B,* diptericin-*lacZ* reporter gene activity of larvae orally infected with *Ecc*15 or *E. coli* strains expressing various Evf derivatives. The following bacterial strains were used: *column 1,* mock; *column 2, Ecc*15 pOM1; *column 3, Ecc*15 *evf*⁻ pOM1; *column 4, Ecc*15 *evf*⁻ pOM1-evf; *column 5, Ecc*15 *evf*⁻ pOM1-evf(C209S); *column 6, Ecc*15 *evf*⁻ pOM1-evf(C209A); *column 7, E. coli* pOM1; *column 8, E. coli* pOM1-evf; *column 9, E. coli* pOM1-evf(C209S); *column 10, E. coli* pOM1-evf(C209A). *Ecc*15 *evf*⁻ or *E. coli* expressing the mutated forms of Evf did not induce expression of the diptericin-*lacZ* reporter gene. Diptericin-*lacZ* activity was monitored in whole larvae 12 h after oral bacterial infection.

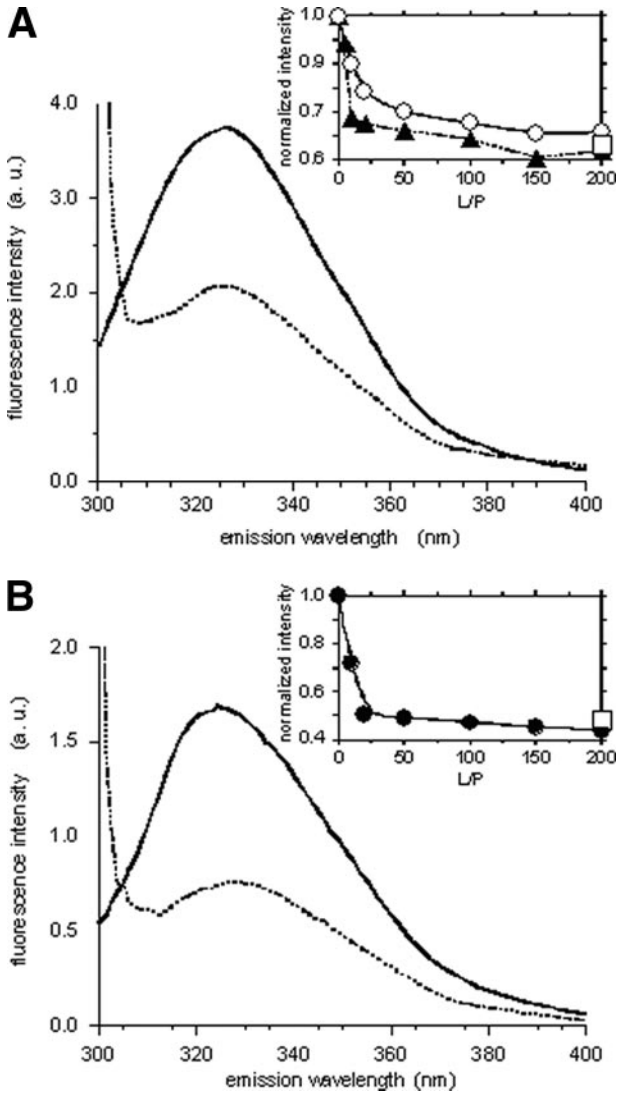

FIGURE 6. **The effect of Evf binding to SUV on the fluorescence emission spectrum of Trp^{94}.** *A,* pH 7.2, *solid line,* 5 μM in buffer; *dotted line,* 5 μM Evf in the presence of SUV (egg PC, lipid/protein ratio = 200, molar ratio). *Inset,* normalized fluorescence intensity as a function of the lipid/protein molar ratio (*empty circles,* egg PC; *filled triangles,* egg PC/POPS 9/1). *B,* pH 5, *solid line,* 5 μM in buffer; *dotted line,* 5 μM Evf in the presence of SUV (egg PC/POPS 80/20 lipid/protein ratio = 200). *Inset,* normalized fluorescence intensity as a function of the lipid/protein molar ratio. The *empty squares* denote measurements after 0.56 M NaCl addition. Excitation wavelength, 298 nm. *a.u.,* arbitrary units.

DISCUSSION

Comparative genomics of bacteria has proven a very effective approach to identify genes involved in pathogenicity. However, few of these pathogenic protein factors were characterized at the biochemical level, and generally their mechanisms of action remain poorly understood. Often the hypothesis on the function of these factors is based on the similarity of their amino acid sequence with those of other proteins of known function. For instance "makes caterpillars floppy" (*mcf*) is the single *Photorhabdus* gene that allows *E. coli* to persist within nematodes (37). *mcf* codes for a 2929-residue protein that has a pro-apoptotic BH3 domain and further resembles *Clostridium difficile* toxin B. Its C terminus is related to the C terminus of apxIVA, an RTX-like toxin from *Actinobacillus pleuropneumoniae*. Therefore, mcf would function as a pro-apoptotic toxin (38).

Evf is a bacterial persistence factor of the *Ecc*15 strain within flies that consists of a 277-amino acid protein that has no sequence similarity with any other protein of known function. To advance our understanding of this virulence factor, we determined its three-dimensional structure. As this revealed that Evf is a protein with a previously unknown fold, the structure cannot be easily used to infer biochemical function. Unexpectedly, the crystal structure revealed the presence of a covalently bound palmitoic acid suggesting that Evf may be targeted to membranes. This observation also provided a handle for experimental exploration. The loss of infectivity for mutants of Cys^{209} that prevent covalent modification strongly suggests that palmitoylation is necessary for biological activity. Covalent attachments of lipids to proteins, such as prenylation, myristoylation, and palmitoylation, are known to play a crucial role in many biological processes. In eukaryotic cells, palmitoylation is a well documented post-translational modification that is involved in membrane localization of soluble proteins, protein-protein interactions, signal transduction, and vesicle transport (39, 40). It should be noted that all the supporting studies of these functions were in eukaryotes; protein palmitoy-

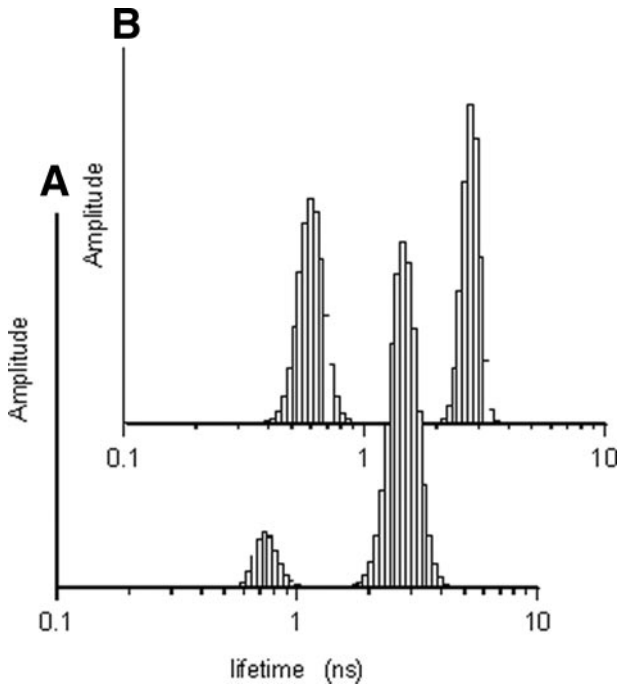

FIGURE 7. **The effect of Evf binding to SUV on the excited state lifetime distribution of Trp^{94}.** *A*, 5 μM Evf in buffer. Fluorescence decay parameters are as follows: $\tau_1 = 2.76$ ns; $\alpha_1 = 0.88$; $\tau_2 = 0.75$ ns; $\alpha_2 = 0.12$; $\langle\tau\rangle = 2.53$ ns. *B*, 5 μM Evf in the presence of SUV (egg PC, lipid/protein ratio = 200). Fluorescence decay parameters are as follows: $\tau_1 = 2.76$ ns; $\alpha_1 = 0.49$; $\tau_2 = 0.60$ ns; $\alpha_2 = 0.51$; $\langle\tau\rangle = 1.70$ ns. The amplitude averaged lifetime is defined as $\langle\tau\rangle = \sum_i \alpha_i \tau_i$.

TABLE 3

The effect of binding of Evf to SUV on the mobility of Trp^{94} measured by fluorescence anisotropy decay

Evf concentration is as follows: 5 μM. Lipid/protein ratio = 1/200 (molar ratio).

Sample	θ_{ns}	$A_{t=0} = \beta$	ω_{max}[a]
			°
Evf, pH 7.2	30 ± 3	0.173 ± 0.007	27 ± 3
Evf, pH 7.2, SUV PC	∞	0.138 ± 0.003	35 ± 2
Evf, pH 7.2, SUV PC/PS 9/1	∞	0.147 ± 0.001	33 ± 1
Evf, pH 7.2, SUV PC/PS 8/2	∞	0.157 ± 0.007	31 ± 3
Evf, pH 5	21 ± 1	0.204 ± 0.001	21 ± 1
Evf, pH 5 SUV PC/PS 9/1	∞	0.131 ± 0.002	37 ± 1
Evf, pH 5, SUV PC/PS 8/2	∞	0.091 ± 0.010	46 ± 3

[a] The semi-angle of the wobbling-in-cone subnanosecond motion was calculated as $\omega_{max} = \text{Arccos}\{1/2((1 + 8(A_{t=0}/A_0)^{1/2})^{1/2} - 1)\}$ (25), with the intrinsic anisotropy $A_0 = 0.251$ (35).

lation or lipidation in general is poorly documented in prokaryotes.

Examination of the structure of Evf provides further arguments in favor of the functional importance of the palmitoylation. Cys^{209} is one of the few totally conserved residues, and the hydrophobicity of the lipid-binding site is also very well preserved, suggesting that palmitoylation must be related to biological function. In line with this hypothesis are our observations that mutants of this cysteine have lost their infectivity. Attempts to overexpress these mutants for biochemical characterization have failed, probably because the modification is necessary to have a stable protein product in solution. The lipid completely fills a very hydrophobic cavity inside the protein, and its absence probably seriously affects stability and/or folding.

Protein palmitoylation is a well documented post-translational modification in eukaryotes that attaches a fatty acid

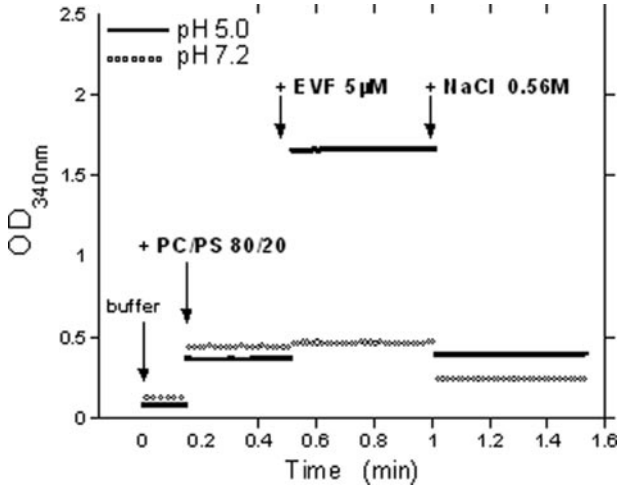

FIGURE 8. **Evf-mediated membrane aggregation.** SUV aggregation was measured by turbidimetry at 340 nm at pH 7.2 (*open circles*) and pH 5 (*black trace*). Lipid/protein ratio = 200.

either through an *N*-amide bond or a thioester (*S*-acylation). In the latter case, the lipid is anchored via a thioester bond to the cysteine sulfur atom. *S*-Acylation is unique in that it is the only reversible modification, which is in agreement with its regulatory function (33). This type of lipid modification is usually on or near amino acid terminal cysteines. In contrast, in Evf the lipid is in a loop at the center of the protein, and it is completely sequestered in a hydrophobic pocket. The buried palmitoyl acid of Evf resembles the yeast protein BET3, a component of the TRAPP complex that is involved in the tethering of transport vesicles to the cis-Golgi membrane (41). BET3 adopts an α/β plait fold that enrolls a hydrophobic pocket burying a palmitate bound through a thioester linkage to a cysteine. BET3 has strong self-palmitoylating activity, and the attached lipid cannot be removed. It was further shown that deacylated BET3 has reduced stability, can no longer form complexes with its protein partner TPC6, and is degraded inside cells (42). It is not known whether Evf has this self-palmitoylating activity or whether it interacts with other protein partners.

The most commonly referenced function of protein palmitoylation is to increase its affinity for lipid membranes thereby affecting its localization. However, Evf did not seem to be associated to the periplasm but instead was present in the cytoplasm (10). Nevertheless, we presume that palmitoylation of Evf is involved in targeting the protein to the plasma membrane. In this respect, we showed that Evf binds to model membranes and promotes their aggregation. Time-resolved fluorescence measurements showed that binding of Evf to lipid vesicles increased the local flexibility of the protein around its sole tryptophan residue. We assume that the palmitoic chain releases from the hydrophobic core upon binding to the vesicles. This would leave an empty channel inside the hydrophobic core of Evf, explaining the increase in tryptophan mobility. The binding was not reversed by ionic strength increase, suggesting that Evf-membrane interactions might be stabilized by hydrophobic anchoring through the palmitoyl moiety. In contrast, membrane aggregation was fully reversed by ionic strength increase, underlying the role of electrostatic interactions in this process. Interestingly, overexpression of Evf promotes bacteria accumu-

lation in the gut. Bacteria in the gut appeared to be present in a regular arrangement that is reminiscent of an organized bacterial community such as biofilm (10). This property of Evf expressing bacteria may be directly linked to the capacity of the Evf protein to interact with and promote aggregation of vesicles. Further work is required to determine how Evf promotes bacteria aggregation in the gut of *Drosophila*.

Pathogenic strains of *E. coli*, *Salmonella*, or *Bordetella* carry palmitoyltransferases in their external membranes (PagP) (43). This enzyme incorporates palmitoic acid into bacterial lipid A, which enables the bacteria to colonize the mucosal environment of their host. PagP is an integral membrane protein, which also incorporates its fatty acid substrate inside the barrel. Plant pathogens *Erwinia* and *Photorhabdus* contain PagP homologues. PagP has a barrel-like architecture shared with another group of well documented soluble lipid-transporting proteins, the lipocallins (44). This architecture is clearly different from that of Evf suggesting that Evf is not a palmitoyltransferase. However, we cannot exclude that Evf modifies in a more subtle way the lipopolysaccharides.

As judged from the full occupancy of the ligand in the crystal structure, recombinant Evf as purified from the bacterial broth is fully palmitoylated. Because no Evf orthologue is present in *E. coli*, palmitoylation most probably has occurred nonenzymatically. It was shown that proteins containing target cysteines can be autoacylated *in vitro* under appropriate conditions in the presence of palmitoyl-CoA (45, 46). Putative acyltransferases have been identified in yeast (42), but none were identified in bacteria. The mechanism of protein palmitoylation on cysteines is poorly documented, but it can be catalyzed by palmitoyltransferases (46). *S*-Palmitoylated proteins have no clear consensus sequence for the modification. It is interesting to note that Evf expressed in *E. coli* carries the palmitoyl modification, although this bacterium is not infectious by itself. Therefore, either Evf is the substrate of a palmitoylating enzyme of *E. coli* or Evf becomes palmitoylated spontaneously during translation. As mentioned for BET3, some proteins are indeed documented to autoacylate in presence of palmitoyl-CoA (47, 48).

In conclusion, the structure of Evf revealed a novel fold and the unforeseen covalent attachment of palmitoic acid to a totally conserved cysteine. These observations and the fact that the cysteine mutant becomes noninfective strongly suggest that the toxic function of Evf is related to this post-translational modification. The biological function of Evf may be related to membrane anchoring of the protein. To our knowledge this is the first well documented example of *S*-palmitoylation on a cysteine for a bacterial protein. Further studies will be necessary to understand the biochemical and cellular significance of this modification.

Acknowledgment—We are grateful to C. Marchand (Institut de Biochimie et de Biophysique Moléculaire et Cellulaire) for mass spectrometry measurements.

REFERENCES

1. Hinnebusch, B. J., Rudolph, A. E., Cherepanov, P., Dixon, J. E., Schwan, T. G., and Forsberg, A. (2002) *Science* **296,** 733–735
2. Beerntsen, B. T., James, A. A., and Christensen, B. M. (2000) *Microbiol. Mol. Biol. Rev.* **64,** 115–137
3. Vallet-Gely, I., Lemaitre, B., and Boccard, F. (2008) *Nat. Rev. Microbiol.* **6,** 302–313
4. Molina, J. J., Harisson, M. D., and Brewer, J. W. (1974) *Am. Pot. J.* **51,** 245–250
5. Kloepper, J. W., Brewer, J. W., and Harrison, M. D. (1981) *Am. Pot. J.* **58,** 165–175
6. Barras, F., van Gijsegem, F., and Chatterjee, A. K. (1994) *Annu. Rev. Phytopathol.* **32,** 201–234
7. Basset, A., Khush, R. S., Braun, A., Gardan, L., Boccard, F., Hoffmann, J. A., and Lemaitre, B. (2000) *Proc. Natl. Acad. Sci. U. S. A.* **97,** 3376–3381
8. Basset, A., Tzou, P., Lemaitre, B., and Boccard, F. (2003) *EMBO Rep.* **4,** 205–209
9. Ellison, D. W., and Miller, V. L. (2006) *Curr. Opin. Microbiol.* **9,** 153–159
10. Acosta Muniz, C., Jaillard, D., Lemaitre, B., and Boccard, F. (2007) *Cell. Microbiol.* **9,** 106–119
11. Hinnebusch, B. J., Perry, R. D., and Schwan, T. G. (1996) *Science* **273,** 367–370
12. Sicard, M., Hering, S., Schulte, R., Gaudriault, S., and Schulenburg, H. (2007) *Environ. Microbiol.* **9,** 12–25
13. Quevillon-Cheruel, S., Collinet, B., Tresaugues, L., Minard, P., Henckes, G., Aufrere, R., Blondeau, K., Zhou, C. Z., Liger, D., Bettache, N., Poupon, A., Aboulfath, I., Leulliot, N., Janin, J., and van Tilbeurgh, H. (2007) *Methods Mol. Biol.* **363,** 21–37
14. Leslie, A. G. W. (1992) *Joint CCP4 + ESF-EAMCB Newsletter on Protein Crystallography, No. 26*, Daresbury Laboratory, Warrington, UK
15. Collaborative Computational Project Number 4 (1994) *Acta Crystallogr. Sect. D Biol. Crystallogr.* **50,** 760–763
16. Grosse-Kunstleve, R. W., and Adams, P. D. (2003) *Acta Crystallogr. Sect. D Biol. Crystallogr.* **59,** 1966–1973
17. Bricogne, G., Vonrhein, C., Flensburg, C., Schiltz, M., and Paciorek, W. (2003) *Acta Crystallogr. Sect. D Biol. Crystallogr.* **59,** 2023–2030
18. Abrahams, J. P., and De Graaff, R. A. (1998) *Curr. Opin. Struct. Biol.* **8,** 601–605
19. Perrakis, A. (1999) *Nat. Struct. Biol.* **6,** 458–463
20. Terwilliger, T. (2004) *J. Synchrotron Radiat.* **11,** 49–52
21. Kleywegt, G. J., and Jones, T. A. (1996) *Acta Crystallogr. Sect. D Biol. Crystallogr.* **52,** 829–832
22. Murshudov, G. N., Vagin, A. A., and Dodson, E. J. (1997) *Acta Crystallogr. Sect. D Biol. Crystallogr.* **53,** 240–255
23. Brochon, J. C. (1994) *Methods Enzymol.* **240,** 262–311
24. Vincent, M., and Gallay, J. (1991) *Eur. Biophys. J.* **20,** 183–191
25. Kinosita, K., Jr., Kawato, S., and Ikegami, A. (1977) *Biophys. J.* **20,** 289–305
26. Tzou, P., Ohresser, S., Ferrandon, D., Capovilla, M., Reichhart, J. M., Lemaitre, B., Hoffmann, J. A., and Imler, J. L. (2000) *Immunity* **13,** 737–748
27. Romeo, Y., and Lemaitre, B. (2008) *Methods Mol. Biol.* **415,** 379–402
28. Leulliot, N., Godin, K. S., Hoareau-Aveilla, C., Quevillon-Cheruel, S., Varani, G., Henry, Y., and van Tilbeurgh, H. (2007) *J. Mol. Biol.* **371,** 1338–1353
29. Leulliot, N., Chaillet, M., Durand, D., Ulryck, N., Blondeau, K., and van Tilbeurgh, H. (2008) *Structure* (*Lond.*) **16,** 52–61
30. Westhead, D. R., Slidel, T. W., Flores, T. P., and Thornton, J. M. (1999) *Protein Sci.* **8,** 897–904
31. Leulliot, N., Quevillon-Cheruel, S., Sorel, I., Graille, M., Meyer, P., Liger, D., Blondeau, K., Janin, J., and van Tilbeurgh, H. (2004) *J. Biol. Chem.* **279,** 23447–23452
32. Liger, D., Quevillon-Cheruel, S., Sorel, I., Bremang, M., Blondeau, K., Aboulfath, I., Janin, J., van Tilbeurgh, H., and Leulliot, N. (2005) *Proteins* **60,** 778–786
33. Nadolski, M. J., and Linder, M. E. (2007) *FEBS J.* **274,** 5202–5210
34. Greaves, J., and Chamberlain, L. H. (2007) *J. Cell Biol.* **176,** 249–254
35. Vincent, M., Gallay, J., Jamin, N., Garrigos, M., and de Foresta, B. (2007) *Biochim. Biophys. Acta* **1768,** 538–552

36. Ichiye, T., and Karplus, M. (1983) *Biochemistry* **22,** 2884–2893
37. Daborn, P. J., Waterfield, N., Silva, C. P., Au, C. P., Sharma, S., and ffrench-Constant, R. H. (2002) *Proc. Natl. Acad. Sci. U. S. A.* **99,** 10742–10747
38. Dowling, A. J., Waterfield, N. R., Hares, M. C., Le Goff, G., Streuli, C. H., and ffrench-Constant, R. H. (2007) *Cell. Microbiol.* **9,** 2470–2484
39. Dunphy, J. T., and Linder, M. E. (1998) *Biochim. Biophys. Acta* **1436,** 245–261
40. Smotrys, J. E., and Linder, M. E. (2004) *Annu. Rev. Biochem.* **73,** 559–587
41. Turnbull, A. P., Kummel, D., Prinz, B., Holz, C., Schultchen, J., Lang, C., Niesen, F. H., Hofmann, K. P., Delbruck, H., Behlke, J., Muller, E. C., Jarosch, E., Sommer, T., and Heinemann, U. (2005) *EMBO J.* **24,** 875–884
42. Lobo, S., Greentree, W. K., Linder, M. E., and Deschenes, R. J. (2002) *J. Biol. Chem.* **277,** 41268–41273
43. Bishop, R. E. (2005) *Mol. Microbiol.* **57,** 900–912
44. Ahn, V. E., Lo, E. I., Engel, C. K., Chen, L., Hwang, P. M., Kay, L. E., Bishop, R. E., and Prive, G. G. (2004) *EMBO J.* **23,** 2931–2941
45. Bizzozero, O. A., Bixler, H. A., and Pastuszyn, A. (2001) *Biochim. Biophys. Acta* **1545,** 278–288
46. Dietrich, L. E., and Ungermann, C. (2004) *EMBO Rep.* **5,** 1053–1057
47. Duncan, J., and Gilman, G. (1996) *J. Biol. Chem.* **271,** 23594–23600
48. Veit, M., Sachs, K., Heckelmann, M., Maretzki, D., Hofmann, K. P., and Schmidt, M. F. (1998) *Biochim. Biophys. Acta* **1394,** 90–98
49. Espeli, O., Moulin, L., and Boccard, F. (2001) *J. Mol. Biol.* **314,** 375–386
50. Gouet, P., Courcelle, E., Stuart, D. I., and Metoz, F. (1999) *Bioinformatics* (*Oxf.*) **15,** 305–308